

Feedback of Tropical Instability-Wave-Induced Atmospheric Variability onto the Ocean

HYODAE SEO

Scripps Institution of Oceanography, La Jolla, California

MARKUS JOCHUM

National Center for Atmospheric Research, Boulder, Colorado

RAGHU MURTUGUDDE

ESSIC/DAOS, University of Maryland, College Park, College Park, Maryland

ARTHUR J. MILLER AND JOHN O. ROADS

Scripps Institution of Oceanography, La Jolla, California

(Manuscript received 27 September 2006, in final form 10 April 2007)

ABSTRACT

The effects of atmospheric feedbacks on tropical instability waves (TIWs) in the equatorial Atlantic Ocean are examined using a regional high-resolution coupled climate model. The analysis from a 6-yr hindcast from 1999 to 2004 reveals a negative correlation between TIW-induced wind perturbations and TIW-induced ocean currents, which implies damping of the TIWs. On the other hand, the feedback effect from the modification of Ekman pumping velocity by TIWs is small compared to the contribution to TIW growth by baroclinic instability. Overall, the atmosphere reduces the growth of TIWs by adjusting its wind response to the evolving TIWs. The analysis also shows that including ocean current (mean + TIWs) in the wind stress parameterization reduces the surface stress estimate by 15%–20% over the region of the South Equatorial Current. Moreover, TIW-induced perturbation ocean currents can significantly alter surface stress estimations from scatterometers, especially at TIW frequencies. Finally, the rectification effect from the atmospheric response to TIWs on latent heat flux is small compared to the mean latent heat flux.

1. Introduction

Tropical instability waves (TIWs) are generated from instabilities of equatorial zonal currents and are a common feature in both the tropical Atlantic (Düing et al. 1975) and Pacific Oceans (Legeckis 1977; Legeckis et al. 1983). Observations reveal TIWs as westward propagating wavelike oscillations of the sea surface temperature (SST) near the equator with a typical wavelength of $\sim 10^\circ$ longitude and a phase speed of $\sim 0.5 \text{ m s}^{-1}$ (Weisberg and Weingartner 1988; Qiao and Weisberg 1995, and references therein). A detailed study of TIWs

is necessary because they are an important element in the momentum balance (Weisberg 1984) and equatorial ocean heat budget (Hansen and Paul 1984; Bryden and Brady 1989; Baturin and Niiler 1997; Jochum and Murtugudde 2006).

Numerous studies have discussed the generation mechanisms and energetics of TIWs. Analytical studies by Philander (1976, 1978) showed that meridional shear of the zonal currents leads to a barotropic conversion of mean kinetic energy to eddy kinetic energy (EKE), which supports the growth of waves with wavelengths and periods similar to those of the observed TIWs. Cox (1980) showed that baroclinic instability, though less important, is also a source of the EKE that is drawn from the mean potential energy. In addition, frontal instability (Yu et al. 1995) and Kelvin–Helmholtz instability (Proehl 1996) were shown to be important EKE

Corresponding author address: Hyodae Seo, Climate Research Division, Scripps Institution of Oceanography, 9500 Gilman Dr., Mail Code 0224, La Jolla, CA 92093.
E-mail: hyseo@ucsd.edu

sources for the TIWs. A more comprehensive numerical study of the generation and the energetics of Pacific TIWs has shown that the northern temperature front is baroclinically unstable, while shear of the zonal currents causes barotropic instability at the equator (Masina et al. 1999, hereafter MPB). These two different instabilities are phase locked and are both important energy sources for TIWs. On the other hand, Jochum et al. (2004, hereafter JMB) found that barotropic instability in the Atlantic was dominant in their energy budget and the baroclinic term was less important.

Chelton et al. (2004) and Xie (2004) demonstrated that ocean–atmosphere interactions involving the oceanic mesoscale occur throughout the World Ocean. SST on this scale induces wind response in the atmospheric boundary layer through modification of the vertical turbulent mixing (Wallace et al. 1989; Hayes et al. 1989). Air over the warm water is destabilized, and increased turbulent mixing of momentum accelerates near-surface winds. Conversely, cold SST suppresses the momentum mixing, decouples the near-surface wind from wind aloft, and hence decreases the near-surface wind. Small et al. (2003) and Cronin et al. (2003) reported that the pressure gradient mechanism of Lindzen and Nigam (1987) is likely to be an important mechanism as well. Furthermore, Chelton et al. (2001) showed that undulating SST fronts by TIWs further affect the perturbation wind stress derivatives in the atmosphere, suggesting a possible feedback from the atmosphere to the TIWs through Ekman dynamics. The lack of simultaneous measurements of ocean currents and wind stresses on the TIW scale makes it difficult to quantify in great detail the feedbacks from the perturbation wind field on the TIWs.

Pezzi et al. (2004) modeled this SST–wind coupling and showed that it reduces variability of TIWs. Their simple coupling parameterization included the effect of TIW-induced SST variations directly on the wind fields and through the modification in wind stress derivatives. Seo et al. (2007) used a full-physics high-resolution regional coupled model to explore several aspects of the tropical Pacific TIWs, reproducing the observed coupling strength as a function of SST gradient.

Recent findings on this close coupling between the ocean and the atmosphere at the oceanic mesoscale raise new questions that have been largely unexplored in the aforementioned studies. What is the role of the wind response in the energy budget of TIWs? How do the atmospheric feedbacks amplify or dampen the TIWs? What is the rectification effect on the mean surface heat flux from the atmospheric response to the TIWs? These questions will be addressed in the present study, which is among the first of its kind using a re-

gional coupled ocean–atmosphere model at eddy-resolving resolution.

In the present study, the regionally coupled high-resolution model of Seo et al. (2007) is used to quantify the contribution of tropical Atlantic ocean–atmosphere covariability to the energetics of the TIWs. It is shown that the direct response of winds to the TIW-induced SST imposes a negative feedback on the growth of TIWs. It is also shown that perturbation Ekman pumping due to TIWs (Chelton et al. 2001) is a very small forcing effect compared to baroclinic instability in the equatorial ocean.

It is also argued that ocean currents (mean + TIWs) substantially reduce the surface stress estimation by 15%–20% over the large area of the South Equatorial Current. Moreover, TIW-induced perturbation ocean currents can significantly alter the local surface stress estimate during the active TIW season. This suggests that numerical studies of TIWs will suffer from a consistency problem when the model is forced with the observed winds such as scatterometer wind stresses.

Last, perturbation latent heat flux generated at the sea surface by evolving TIW–SST is small compared to the contribution from the mean component, indicating only a weak rectification effect on the ocean from these high-frequency perturbations.

In section 2, the model and experiment designed for this study are explained. In section 3, the main results of the study are discussed, followed by the conclusions and summary in section 4.

2. Model and experiment

The coupled model used for the present study is the Scripps Coupled Ocean–Atmospheric Regional (SCOAR) model (Seo et al. 2007). It combines two well-known, state-of-the-art regional atmosphere and ocean models using a flux–SST coupling strategy. The atmospheric model is the Experimental Climate Prediction Center (ECPC) Regional Spectral Model (RSM) and the ocean model is the Regional Ocean Modeling System (ROMS).

The RSM, originally developed at the National Centers for Environmental Prediction (NCEP) is described in Juang and Kanamitsu (1994) and Juang et al. (1997). The code was later updated with greater flexibility and much higher efficiency (Kanamitsu et al. 2005; Kanamaru and Kanamitsu 2007). Briefly, it is a limited-area primitive equation atmospheric model with a perturbation method in spectral computation, and utilizes a terrain-following sigma coordinate system (28 levels). The model physics are the same as for the NCEP global seasonal forecast model (Kanamitsu et al. 2002a) and

NCEP–National Center for Atmospheric Research (NCAR) reanalysis model (Kalnay et al. 1996) except for the parameterization of convection and radiative processes.

The ROMS solves the incompressible and hydrostatic primitive equations with a free surface on horizontal curvilinear coordinates and utilizes stretched generalized sigma coordinates in order to enhance vertical resolution near the sea surface and bathymetry. The details of the model can be found in Haidvogel et al. (2000) and Shchepetkin and McWilliams (2005).

A flux–SST coupler bridges the atmospheric (RSM) and ocean (ROMS) models. The coupler works in a sequential fashion; the RSM and ROMS take turns integrating while exchanging forcing every 24 h. The interacting boundary layer between RSM and ROMS is based on the bulk formula for surface fluxes of momentum and sensible and latent heat adapted from the algorithm of Fairall et al. (1996).

Although the drag coefficient is generally a function of both wind speed and atmospheric boundary layer stability, Liu et al. (1979) showed that, for the typical environmental conditions in the Tropics, with near-surface wind speeds of $\sim 7 \text{ m s}^{-1}$, the bulk transfer coefficients are only marginally sensitive to the typical changes in the stability induced by $\pm 0.5^\circ\text{C}$ changes in air – sea temperature difference. Thus, bulk transfer coefficients for momentum and the moisture remain largely unchanged by the changes in the atmospheric stability due to TIW–SST changes.

Seo et al. (2006) showed that resolving mesoscale variability in the equatorial Atlantic Ocean is important in improving the simulations of large-scale mean SST and the precipitation. The present study uses the identical model setup as in Seo et al. (2006), except for an enhanced atmospheric resolution of $\sim 1/4^\circ$ to match the underlying ocean grid at $\sim 1/4^\circ$. Comparable high resolution in the coupled model allows for synchronous local feedback of ocean and atmosphere arising in the presence of ocean mesoscale eddies including TIWs.

The initialization and forcing procedures for both cases are as follows. The ROMS ocean was first spun up for 8 years with the Comprehensive Ocean–Atmosphere Dataset (COADS) climatological atmospheric forcing (da Silva et al. 1994) and climatological oceanic boundary conditions from the *World Ocean Atlas 2001* (Conkright et al. 2002). Then the SCOAR coupled run was launched for 7 years from 1998 to 2004 with low-wavenumber NCEP/Department of Energy (DOE) reanalysis II (Kanamitsu et al. 2002b) atmospheric forcing and climatological oceanic boundary conditions. The 6-yr solution from 1999 to 2004 is analyzed in this study.

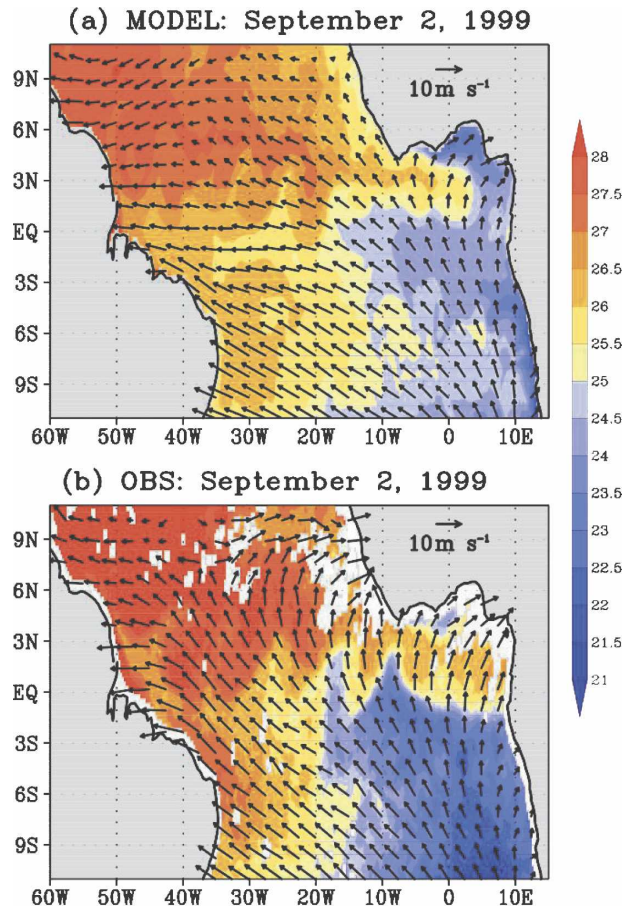


FIG. 1. Three-day-averaged SST and 10-m winds centered on 2 Sep 1999 (a) in the model and (b) from the satellite of the TMI tropical instability waves and the QuikSCAT scatterometers. The TIWs are shown as undulations of the SST front near the equator. The TRMM SST and the QuikSCAT wind vectors are regridded to the model grid in (a). The vectors are shown on every 10 (5) grid points in x (y).

The model domain covers the whole tropical Atlantic basin from 30°S to 30°N , 70°W to 20°E including eastern Brazil and western Africa. Since the focus of the present study is the effect of atmospheric feedbacks on TIWs, the domain analyzed here is limited to the region close to the equator where TIW activity is large. Figure 1 shows a snapshot of SST that represents the typical spatial patterns of TIWs from the model, in comparison to measurements from the Tropical Rainfall Measuring Mission (TRMM) Microwave Imager (TMI). The simulated TIWs in the model are qualitatively similar to the observations, with cusps of SST north of the equator along the equatorial front. However, an exact correspondence of the modeled TIWs with the observations at any given time is not expected because TIWs are generated by internal ocean dynamics, rather than deterministically forced. On the other

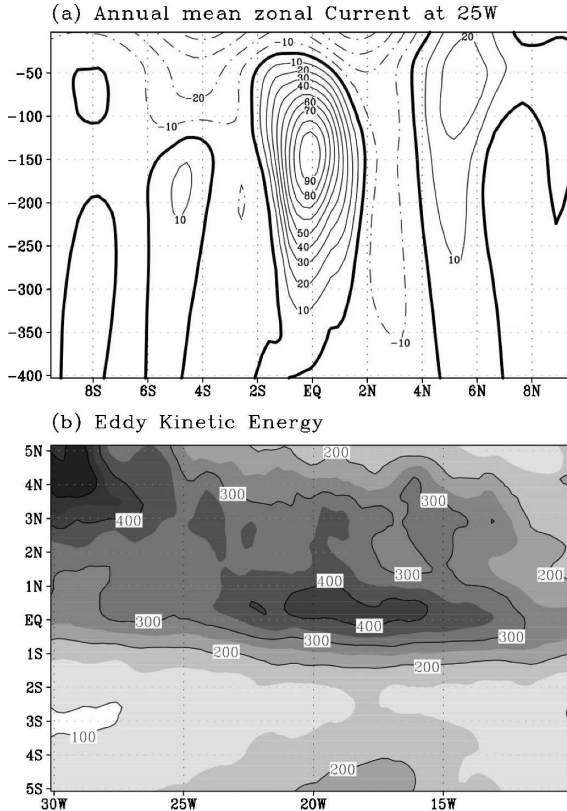


FIG. 2. (a) Six-year model mean (1999–2004) zonal current along 23°W . The westward South Equatorial Current is shown by dashed contour lines. Zero values are shown in thick contours. The core of the equatorial undercurrent is located at 150-m depth. Tsuchiya jets are shown as the eastward subsurface currents centered at 5°N and 5°S . (b) Near-surface model EKE computed by $\text{EKE} = (u'^2 + v'^2)/2$, where u' and v' are zonally high-pass-filtered surface currents. The maximum EKE is located north of the equator along the core of the TIWs.

hand, the eddy statistics of the waves are well represented in the SCOAR model (Fig. 2b).

Figure 2 shows an annual-mean zonal current at 23°W and the EKE of the near-surface currents. The core of the equatorial undercurrent (EUC) reaching $\sim 100 \text{ cm s}^{-1}$ is located at a depth of 150 m, and this compares well with the observations (e.g., Brandt et al. 2006; Schott et al. 2003) and modeling studies (JMB). The maximum EKE, greater than $400 \text{ cm}^2 \text{ s}^{-2}$ is located at the equator, which is also consistent with time-mean perturbation kinetic energy estimated from the observations (Weisberg and Weingartner 1988).

Temporal filtering of data is useful to extract the characteristics of the TIWs (e.g., Hashizume et al. 2001; JMB). However, temporal bandpass filtering alone (e.g., 10–40 days) does not completely rid the system of intrinsic higher frequency (3–15 days) synoptic variability in the atmosphere. A spatial (zonal) filtering in com-

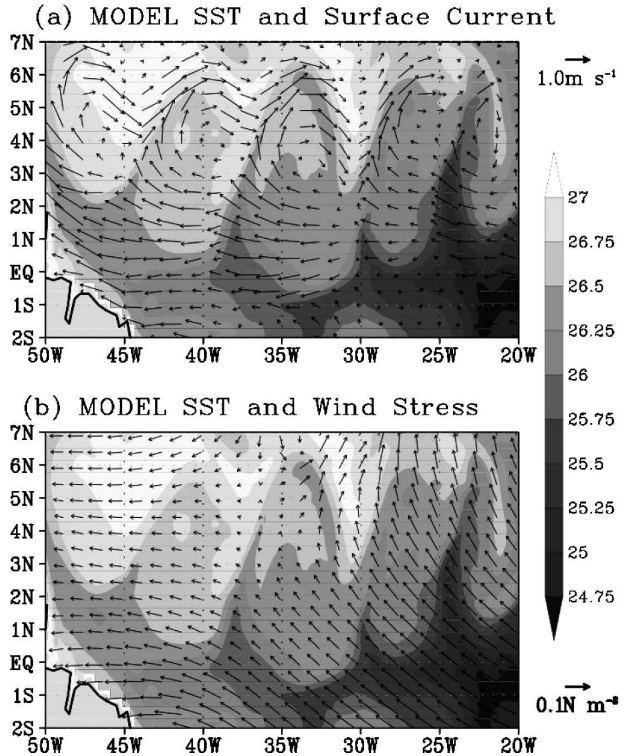


FIG. 3. Three-day-averaged model SST fields centered on 26 Sep 2000 with vectors of (a) the model surface current (m s^{-1}) and (b) the model wind stress (N m^{-2}). The vectors are shown on every 5 (2) grid points in x (y).

bination with some temporal smoothing is more useful when one aims to highlight covarying patterns of the ocean–atmosphere signals arising from fast-moving TIWs (e.g., Chelton et al. 2001; Small et al. 2003). Thus, all the variables analyzed in this study are zonally high-pass filtered to retain the signals of the ocean and the atmosphere less than 10° longitude and also 5-day averaged to reduce the fast-changing atmospheric and oceanic variability.

3. Result

a. Impact of wind current covariability on the TIWs

Figure 3 shows a snapshot of TIW–SST overlaid with surface currents and wind stresses. Anticyclonic ocean currents are generated north of the equator in association with TIWs (Fig. 3a), over which large-scale winds are southeasterly, traversing the SST front (Fig. 3b). Figure 4 shows a 3-day-averaged snapshot of SST anomaly, SST' , overlaid with the perturbation surface currents, \mathbf{u}' , and wind stresses, $\boldsymbol{\tau}'$, associated with the TIWs. SST' and $\boldsymbol{\tau}'$ have an in-phase relationship, such that warm (cold) SST' enhances (reduces) southeast-

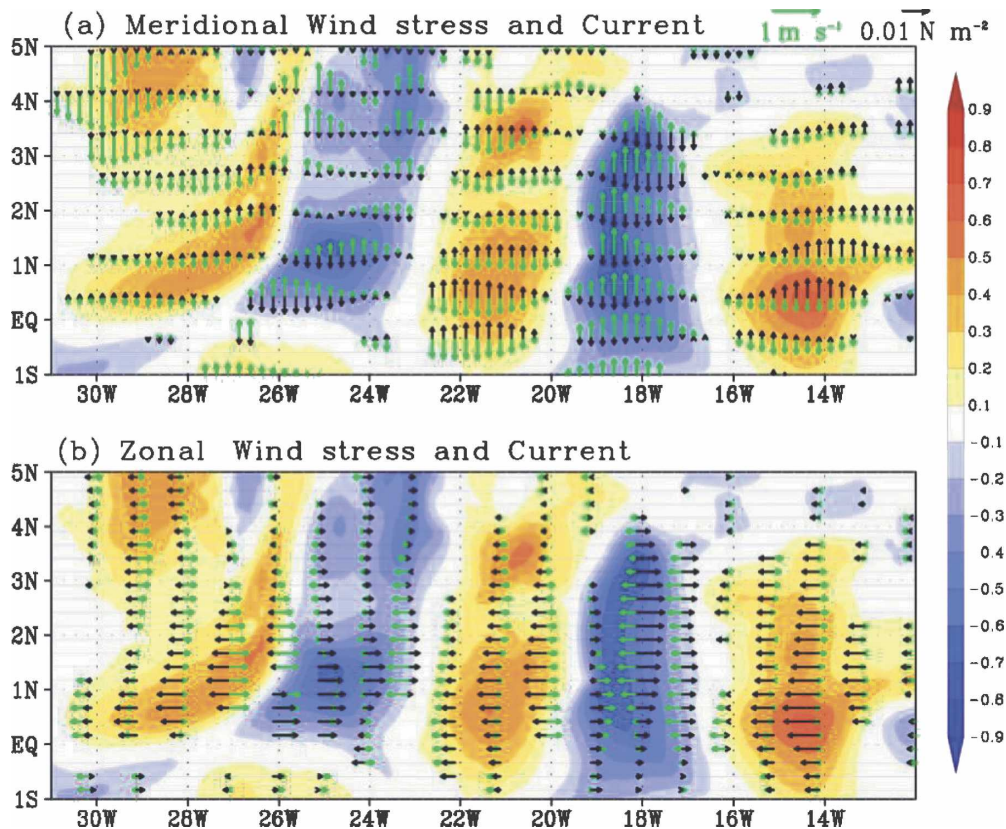


FIG. 4. Three-day-averaged (centered on 22 Oct 2000) and high-pass-filtered model SST (color shaded) overlaid with high-pass-filtered model surface current (green vectors), and model wind stress (black vectors) in the (a) meridional and (b) zonal components.

erly background atmospheric flows. This is a result of changes in stratification of the lower atmospheric boundary layer according to the underlying SST', which in turn leads to the atmospheric adjustment of vertical turbulent mixing of momentum (Wallace et al. 1989; Hayes et al. 1989).

Apparent in Fig. 4 is that τ' is generally in the opposite direction of \mathbf{u}' , particularly for the meridional components in Fig. 4a. Figure 5 shows a simple schematic representation of such a relationship. Cold, newly upwelled waters from the equator are pushed northward by TIWs while they drive warm water from the north equatorward (Fig. 3a). The anomalous meridional currents are slowed down by perturbations in meridional surface winds, which are generated in response to the TIW–SST. This feedback results in a significant negative correlation north of the equator where TIWs are most energetic (Fig. 6a). The significant positive correlation south of the equator can be understood similarly.

The relationship between the zonal TIW perturbation currents and wind stresses is more complicated because of asymmetric responses in the southern and northern part of the TIW–SST. In the northern flank of

the eddy (Figs. 4b and 5b), the above explanation is true, where zonal wind stress and zonal surface current generally oppose each other. This is because warm SST increases the easterly background winds where TIWs generate eastward currents (Fig. 3a). Near the equator, however, a significant positive correlation indicates that winds and currents are aligned together zonally. This results when the warm water pushed by TIWs from the north turns westward at the equator to close the anticyclonic ocean eddy over which easterly winds are accelerated (Figs. 3a and 4b). Figure 6b shows bands of positive correlation near the equator and negative correlation north of the equator. We now discuss how these correlation patterns translate into the EKE budget of the TIWs.

Here we use a similar technique as used by MPB and JMB, based on the EKE budget. The difference is that in their equation the eddy component is defined as a deviation from the time-mean flow, whereas here it is defined as a deviation from the 10° longitude zonal running mean averages. In the Pacific Ocean, a longer cutoff wavelength could be used in bandpass filtering, while this is not desirable in the tropical Atlantic Ocean

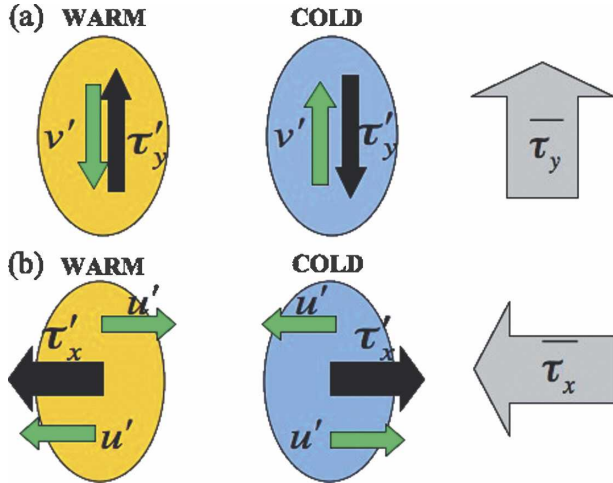


FIG. 5. Schematic representation of the relationship between wind stress and surface current over TIW-SST. Warm (cold) TIW-SST is shown as light yellow (blue) ovals. Black (green) vectors are perturbation wind stress (surface current). Background wind fields are shown as thick gray vectors.

because the basin is much smaller and this would give rise to more ocean grid points lost from the continental boundary. It should be noted, however, that the results discussed here are not significantly altered by the choice of cutoff wavelength of the zonal filter, so long as the TIW signals are retained.

MPB estimated each term of the EKE budget in the tropical Pacific Ocean using a numerical ocean model. The EKE equation can be written as

$$\begin{aligned} \mathbf{U} \cdot \nabla \mathbf{K}_e + \mathbf{u}' \cdot \nabla \mathbf{K}_e &= -\nabla \cdot (\mathbf{u}' p') - g \rho' w' \\ &+ \rho_o [-\mathbf{u}' \cdot (\mathbf{u}' \cdot \nabla \mathbf{U})] \\ &+ \rho_o A_h \mathbf{u}' \cdot \nabla^2 \mathbf{u}' + \rho_o \mathbf{u}' \cdot (A_v \mathbf{u}'_z)_z \\ &+ \mathbf{u}'_{\text{sfc}} \cdot \boldsymbol{\tau}'_z. \end{aligned} \quad (1)$$

The capital letters denote the annual-mean values and the primes are zonally bandpass-filtered values. Here \mathbf{K}_e is the EKE; (u, v, w) the ocean velocity vector components; p the pressure; ρ the density; g the gravitational acceleration; A_h and A_v are the horizontal and vertical viscosities, respectively; and $\boldsymbol{\tau}$ is the surface wind stress. The terms on the lhs are horizontal and vertical advectations of EKE by the mean and eddy currents. The annual-mean local tendency of the EKE is negligible. The first term on the rhs is the vertical and horizontal radiation of energy, and the second term represents a baroclinic conversion process, whereby mean available potential energy is converted into EKE. The third term is the horizontal deformation work that represents a conversion from mean kinetic energy to

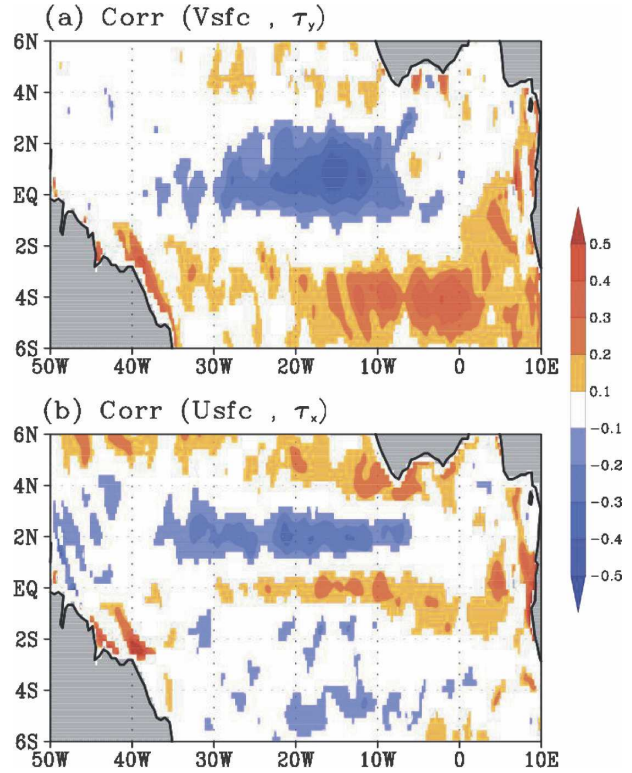


FIG. 6. Map of correlation of 6-yr high-pass-filtered model wind stress and surface current over the tropical Atlantic Ocean in the (a) meridional and (b) zonal directions.

EKE. The fourth and fifth terms designate the horizontal and vertical dissipation, respectively, of EKE by the eddies. The last term, which is the focus of the present study, corresponds to the effect of the correlation of currents and wind stresses integrated to the depth at which momentum input from wind stress vanishes.

From the estimates of each term of Eq. (1) using their model output, JMB concluded that barotropic conversion of the zonal flow, the component, $-\rho_o(u'v'U_y)$, of the full term, $\rho_o[-\mathbf{u}' \cdot (\mathbf{u}' \cdot \nabla \mathbf{U})]$, was the dominant source for the TIW EKE. Other deformation terms in the barotropic convergence rate, $-\rho_o(u'u'U_x + u'v'V_x + v'v'V_y)$, and the baroclinic conversion rate, $-g\rho'w'$, were argued to be less important.

For the previous studies of the energetics of TIWs, including MPB and JMB, the effect of the correlation between ocean surface currents and wind stresses, the last term of Eq. (1), was zero by construction because their models were forced with climatological wind. Vertical averaging of Eq. (1) gives an estimate of the relative importance of this term, $\mathbf{u}'_{\text{sfc}} \cdot \boldsymbol{\tau}'_z$, compared with, for example, the barotropic convergent rate of the zonal flow, $-\rho_o(u'v'U_y)$. Figure 7 shows the 6-yr mean and zonal-mean $\rho_o(u'v'U_y)$ and $\mathbf{u}'_{\text{sfc}} \cdot \boldsymbol{\tau}'_z$ averaged from

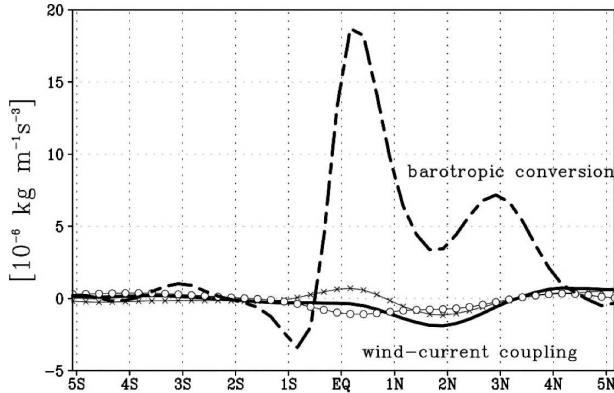


FIG. 7. Zonal average (30° – 10° W) of the 6-yr model mean (dashed line) barotropic conversion rate of the zonal flow, $-\rho_o(u'v'U_y)$ averaged over 150 m, i.e., $d^{-1}\int_d^{sfc}(-\rho_o u'v'U_y) dz$, where d is the depth of the center of EUC (150 m). (Solid line) Time- and zonal-mean $\mathbf{u}'_{sfc} \cdot \boldsymbol{\tau}'_z$ averaged over 150 m, i.e., $d^{-1}\int_d^{sfc}(\mathbf{u}'_{sfc} \cdot \boldsymbol{\tau}'_z) dz$. Zonal (meridional) component of $d^{-1}\int_d^{sfc}(\mathbf{u}'_{sfc} \cdot \boldsymbol{\tau}'_z) dz$ is shown by the light solid line with x (o).

the surface to 150-m depth. This depth range should include the maximal effects of both of these terms. For example, the center of the EUC is located at 150-m depth (Fig. 2a) where $-\rho_o(u'v'U_y)$ is most dominant (JMB). Wind input, in contrast, should be largest near the surface and decrease to small values near the center of the EUC.

The magnitude of the time- and zonal-mean barotropic conversion of the zonal flow, $-\rho_o(u'v'U_y)$, in the present model compares well with the estimate of JMB, although there is a secondary peak at 3° N, which was not seen in their study. The sign of the energy conversion rate estimated in each direction agrees with the map of correlation. Positive correlation of zonal winds and currents (Fig. 6b), for example, results in an EKE source at the equator (Fig. 7). Overall, the net impact of the correlation of \mathbf{u}' and $\boldsymbol{\tau}'$ is largely negative, with its peak at 2° N. At this particular latitude, the wind contribution to the TIW energy budget is large, amounting to roughly 40% of the barotropic convergent rate term. If averaged over TIW region (2° S– 5° N), the contribution from wind–current coupling is $\sim 10\%$ of the barotropic conversion term, which suggests that overall wind–current coupling is a small but significant sink of EKE of the TIWs. This is one of the main results of this study. This agrees with the observational study by Polito et al. (2001) who showed, based on the analysis of TIW anomaly relationship using the satellite data and assuming geostrophy, that meridional wind speeds are in quadrature with sea surface heights, and thus in opposition to the phase of meridional TIW currents. This implies that the opposing winds slow down the surface current associated with the TIWs.

In addition to the feedback arising from a direct response of winds to TIWs, Chelton et al. (2001) found that perturbation wind stress curl generated at the front by TIWs could be an additional feedback. Spall (2007) discussed how the observed relationship of SST and wind stresses affects the baroclinic instability of the ocean through Ekman pumping. Then he applied this model to a classic linear, quasigeostrophic stability problem for a uniformly sheared flow originally studied by Eady (1949). For the case of southerly background winds blowing from cold to warm waters, his analysis indicates that Ekman pumping and the forced vorticity would reduce the growth rate and wavelength of the most unstable wave (Fig. 1 of Spall 2007).

In the current model, the effect of Ekman pumping on the TIWs is estimated by comparing the magnitudes of Ekman pumping velocity, w'_e , and perturbation vertical velocity, w' , from the model output which enters the baroclinic conversion term [Eq. (1)]. This w' is computed at the base of the mixed layer, which is defined as depth at which SST decreases by 0.5° C from the sea surface. In Fig. 8, Hovmöller diagrams of w' and w'_e at 2° N for one particular TIW season (mid-May 2001 to January 2002) illustrate the westward propagating features of both w' and w'_e , although w' exhibits more coherent spatial structures that resemble TIWs with much stronger amplitudes. Time series of w' and w'_e at 2° N, 30° W confirm that the amplitudes of w' are much stronger than those of w'_e throughout the whole 6-yr period.

This suggests that the effect of wind stress curl due to the zonal SST gradient is a minor contribution to the TIWs compared to the baroclinic energy source intrinsic to the ocean. However, this result comes with the caveat that Ekman pumping velocity becomes singular at the equator and the variability in upwelling due to direct wind effects is difficult to quantify.

Hence, the net effect of the two sources of atmospheric feedback (i.e., a direct response of wind and Ekman pumping) due to TIW–SST weakly damps the TIWs. This is consistent with the results by Pezzi et al. (2004) who parameterized this feedback effect by adding an empirical correlation between SST and surface wind to the forcing fields of their ocean general circulation model (OGCM).

b. Impact of surface current on wind stress

The Quick Scatterometer (QuikSCAT) measures wind stresses at the sea surface from the intensity of the backscatter in the Ku band (Kelly et al. 2001). This stress is a function of the ocean surface state, including roughness, as well as atmospheric background winds (Chelton and Freilich 2005). Kelly et al. showed that

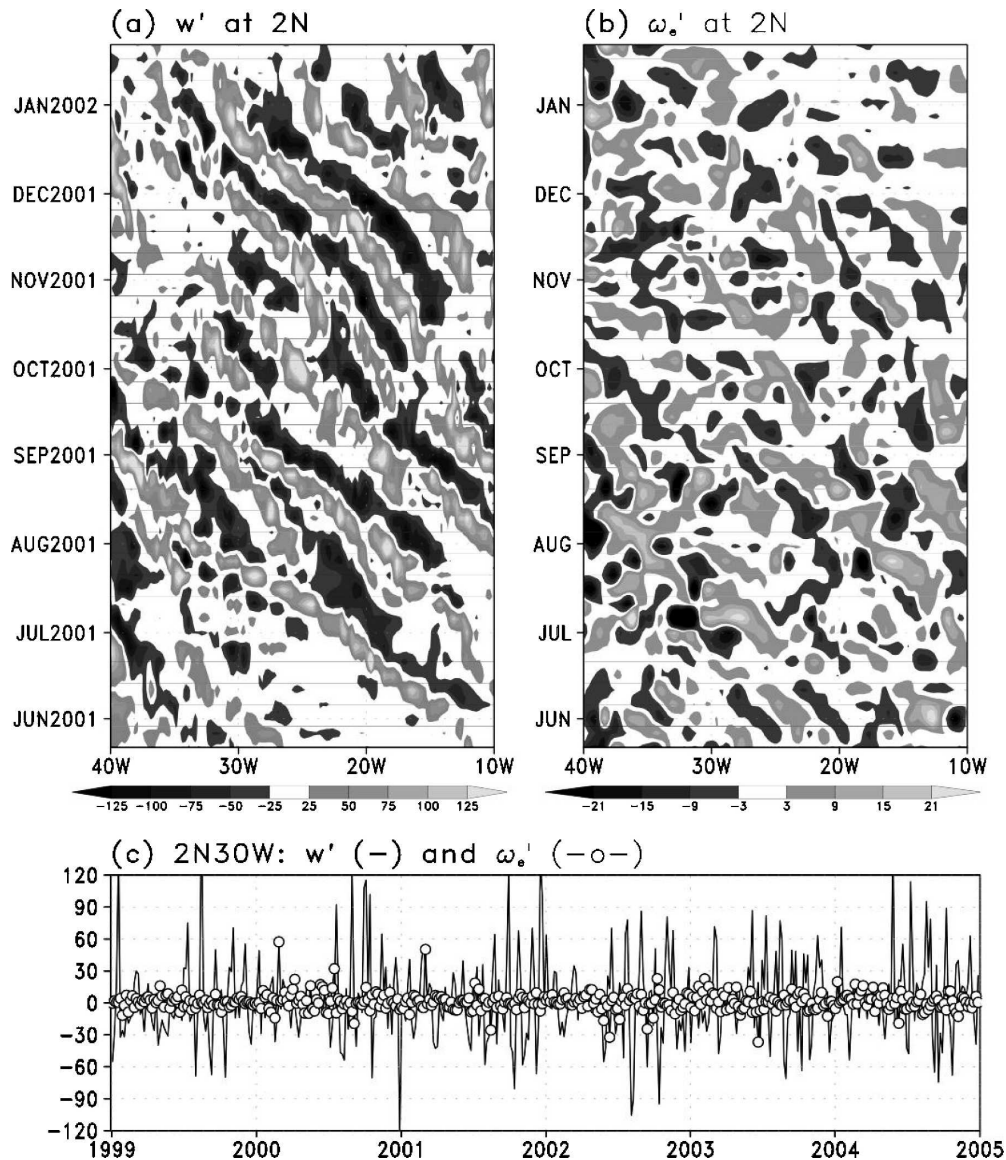


FIG. 8. Hovmöller diagrams of (a) the model perturbation vertical velocity w' , evaluated at the base of the mixed layer ($\sim 40\text{--}50$ m), from the baroclinic convergent rate term ($-g\rho'w'$) and (b) the model Ekman pumping velocity, ω_e' , at 2°N from mid-May 2000 to January 2001. (c) Times series of w' (solid) and ω_e' (line with o) at 2°N, 30°W. Note the different color scales in (a) and (b). Time axis of (a) and (b) denotes January of the year.

the difference of mean winds from the QuikSCAT and the Tropical Atmosphere–Ocean (TAO) array closely resembles the mean equatorial surface currents, and this is attributed to the QuikSCAT measuring the relative motion of air and sea.

Here the effect of TIW-induced surface currents on the surface wind stress estimation is examined. The surface wind stresses are computed for the different scenarios with the knowledge of the model 10-m winds and the ocean surface current using bulk formulae. The

wind stress parameterization of QuikSCAT can be written as

$$\tau_1 = \rho C_d |\mathbf{u}_a - \mathbf{u}_o| (\mathbf{u}_a - \mathbf{u}_o), \quad (2)$$

where ρ is the air density, C_d is the drag coefficient (1.3×10^{-3}), \mathbf{u}_a is the atmospheric wind velocity, and \mathbf{u}_o is the ocean surface current velocity. Thus $|\tau_1|$ is an estimated surface stress magnitude in the presence of the surface ocean current (mean currents + TIW currents).

If the ocean surface were motionless, the wind stress, τ_2 , is written as

$$\tau_2 = \rho C_d |\mathbf{u}_a| \mathbf{u}_a. \quad (3)$$

If the effect of TIW currents on wind stresses is removed by a zonal low-pass filter, this wind stress, τ_3 , can then be written as

$$\tau_3 = \rho C_d |\mathbf{u}_a - \mathbf{u}_{o_lowpass}| (\mathbf{u}_a - \mathbf{u}_{o_lowpass}), \quad (4)$$

where $\mathbf{u}_{o_lowpass}$ is the low-passed surface current velocity to remove the TIW currents. Comparison of $|\tau_1|$ and $|\tau_2|$ gives an estimate of the effect of ocean currents on the surface wind stresses. Comparison of $|\tau_1|$ and $|\tau_3|$ will show the effect of TIW-induced perturbation ocean currents on the surface wind stresses. Figure 9a shows a time series of $|\tau_1|$ at 2°N averaged over 20° and 15°W, where the TIW activity is large. The time series of $|\tau_1|$ exhibits a strong intraseasonal variability, in particular during the second half of the year when TIWs are active. The annual-mean wind stress over this area is roughly 0.027 N m^{-2} .

Figure 9b shows that $|\tau_1| - |\tau_2|$ is mostly negative, with a larger deficit in $|\tau_1|$ in the second half of each year. This indicates that including ocean currents reduces the wind stress estimate at this latitude (2°N) evidently because the mean South Equatorial Current is in the same direction as the large-scale winds. This is consistent with the results of Kelly et al. (2001). Figure 10a shows the map of the annual-mean $(|\tau_1| - |\tau_2|)/|\tau_1|$. Over the large area across the equator and the coastal regions, the effect of the ocean surface current is to reduce the surface stress by 15%–20% in the current model, consistent with the previous studies (Pacanowski 1987; Luo et al. 2005; Dawe and Thompson 2006). Even larger values found at the coastal oceans suggest that strong variability of the coastal currents can significantly alter the estimated surface stresses near the coast.

Figure 9c shows a 6-yr time series of $|\tau_1| - |\tau_3|$, which closely resembles TIW currents in the ocean (Fig. 9d, with correlation coefficient of -0.8). This shows the importance of fluctuating ocean currents on the estimation of wind stress. Since the annual mean of $|\tau_1| - |\tau_3|$ is close to zero because of the oscillatory cancellation of the TIW currents, the annual-mean TIW currents do not significantly affect the annual-mean surface wind stress estimates. However, it should be noted that during the active season of the TIWs, TIW currents substantially modify the estimate of the surface wind stress. Figure 10b shows one example from the 5-day-averaged fields centered on 23 June 2000 in the model. The spatial map of $(|\tau_1| - |\tau_3|)/|\tau_1|$ demonstrates the alternat-

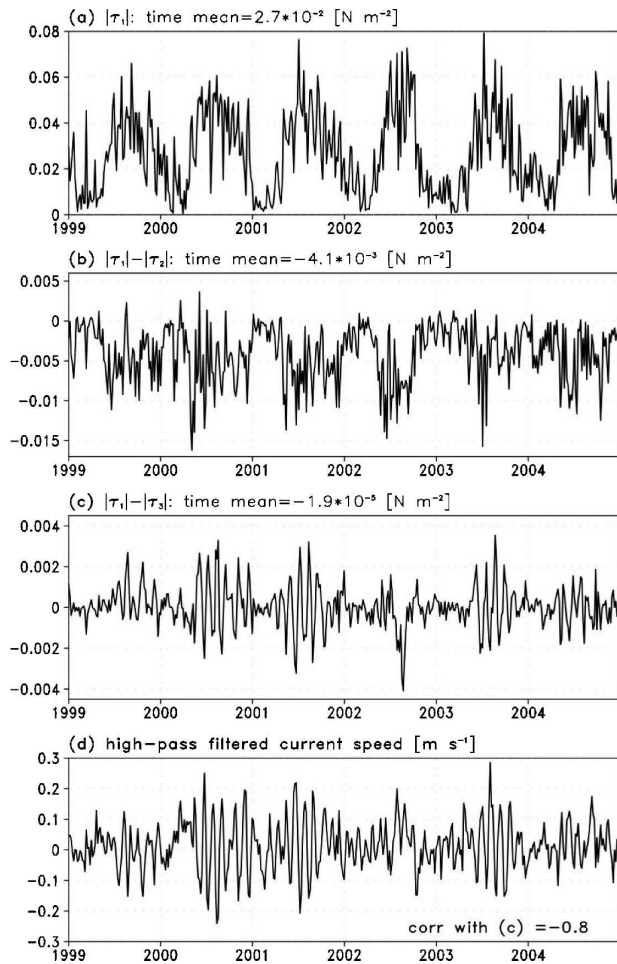


FIG. 9. Six-year time series of model surface wind stress magnitudes computed for the different scenarios at 2°N averaged over 20° and 15°W for (a) $\tau_1 = \rho C_d |\mathbf{u}_a - \mathbf{u}_o| (\mathbf{u}_a - \mathbf{u}_o)$, (b) $|\tau_1| - |\tau_2|$ in which $\tau_2 = \rho C_d |\mathbf{u}_a| \mathbf{u}_a$, and (c) $|\tau_1| - |\tau_3|$, where $\tau_3 = \rho C_d |\mathbf{u}_a - \mathbf{u}_{o_lowpass}| (\mathbf{u}_a - \mathbf{u}_{o_lowpass})$; \mathbf{u}_a is the atmospheric wind velocity, \mathbf{u}_o is the ocean surface current velocity (mean + TIWs), $\mathbf{u}_{o_lowpass}$ is the low-passed surface current velocity. (d) High-pass-filtered (TIW) surface current speed (m s^{-1}). The correlation coefficient of the TIW current speed with $|\tau_1| - |\tau_3|$ in (c) is -0.8 . See text for details.

ing bands of positive and negative contribution from the TIW-induced perturbation currents. During this particular period, the effect of TIW currents on the surface stress can be $\pm 25\%$ – 30% . Considering the alternating phases of the waves, the peak-to-trough difference is perhaps even larger. The higher $(|\tau_1| - |\tau_3|)/|\tau_1|$ ratio ($< -40\%$) near the coast suggests that mesoscale current variability associated with oceanic ring formation in the north Brazil Current (Johns et al. 1998) can be of substantial importance to the surface stress estimation in this region.

A large influence of the perturbation ocean current on the surface stress estimation implies a potential

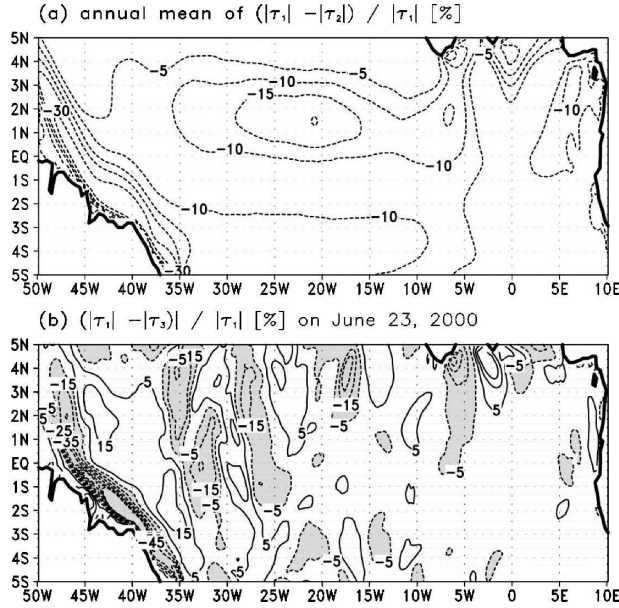


FIG. 10. (a) Map of the ratio (%) of annual-mean $(|\tau_1| - |\tau_2|) / |\tau_1|$. Negative values denote the reduction of the wind stress estimate due to the presence of ocean surface currents. (b) The 5-day-averaged (centered on 23 Jun 2000) ratio, $(|\tau_1| - |\tau_3|) / |\tau_1|$. Negative values are shaded in gray and contoured in dashed lines; contour interval is 5% and the zero contour line is omitted.

problem in those numerical ocean modeling studies where the QuikSCAT-derived wind stress product is prescribed at the sea surface. In reality and in the SCOAR model, TIWs induce intraseasonal variability in the atmospheric wind field, whereas in OGCMs forced with high-frequency wind fields TIWs occur with random phases and will, in general, be mismatched with specified local surface winds. The large alteration of surface stress by the TIW currents suggests that, in these forced models, the estimation of surface stress may be significantly misestimated, leading to a possible source of error associated with this coupled feedback.

c. Implication of TIW-induced latent heat flux on SST

Observational studies have revealed a negative impact from the perturbation surface heat flux on the evolving SST of TIWs. Deser et al. (1993) found a correlation between SST and stratocumulus cloudiness where increased cloudiness over warm SST reduces incoming solar radiation flux, thus cooling the SST. Numerous investigators (e.g., Thum et al. 2002; Liu et al. 2000; Zhang and McPhaden 1995) have shown that increased latent and sensible heat flux is found over the warm phase of TIWs due to strong coupling between

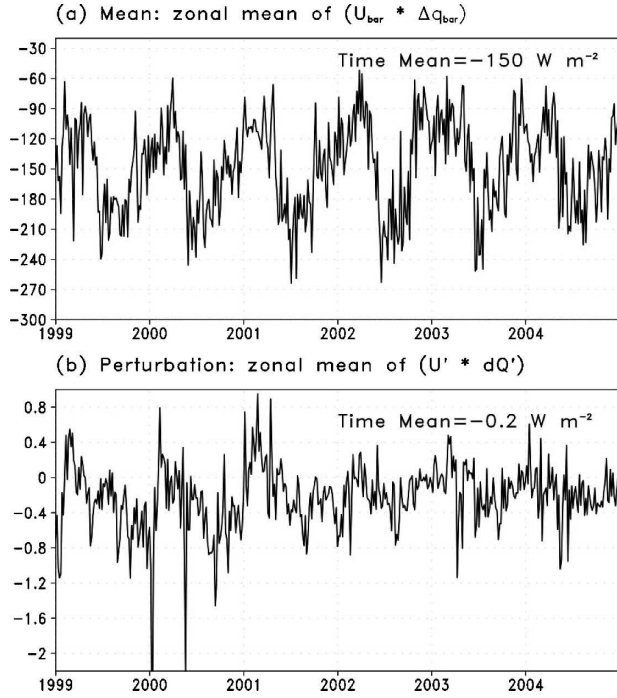


FIG. 11. Six-year time series of (a) $\rho L C_H \overline{U \Delta q}$ and (b) $\rho L C_H \overline{U' \Delta q'}$ at 2°N averaged over 30°–10°W in the model. Similar results are found for different areas.

SST and winds, which dampens the growth of the TIWs. Here we examine how the perturbation latent heat flux generated by TIWs compares with the zonal-mean latent heat flux, that is, the rectifying effect from perturbation heat flux to the mean SST.

In the bulk parameterization (Fairall et al. 1996), latent heat flux (LH) can be written as

$$\text{LH} = \rho L C_H U (\Delta q), \quad (5)$$

where ρ is the density of air, L the latent heat of vaporization of water, C_H the bulk exchange coefficient, U is the wind speed, and Δq is the difference between the specific humidity of air and the saturation specific humidity at the temperature of the ocean surface. Thus LH is proportional to the product of U and Δq . Reynolds averaging yields

$$\overline{\text{LH}} = \rho L C_H (\overline{U \Delta q} + \overline{U' \Delta q'}), \quad (6)$$

where the overbar denotes a 10° longitude running mean and the primes denote deviations from the zonal running mean. Thus, zonally averaged latent heat flux in the equatorial ocean is determined both from the zonal mean and the deviation of the product of wind and humidity differences. Figure 11 shows a 6-yr time

series of the mean and deviation component of latent heat flux at the representative region 2°N averaged over 30°–10°W. The time average of the mean latent heat flux at this latitude is roughly -150 W m^{-2} . The deviation can reach $\sim 1\%$ – 2% of the mean, but is generally small compared to the mean. This implies that rectification from the perturbation latent heat flux onto the heat budget in the equatorial ocean is close to zero.

Zhang and McPhaden (1995) found that a 1-K change in SST due to TIWs creates a latent heat flux anomaly of $\sim 50 \text{ W m}^{-2}$ in the eastern Pacific Ocean. Seo et al. (2007) found comparable values for perturbations of latent heat flux [$34 \text{ W m}^{-2} (1 \text{ K SST})^{-1}$] in their eastern Pacific TIW model. The current model agrees with these estimates in the eastern Pacific and generates approximately 25 W m^{-2} changes in latent heat flux due to the 1 K change in TIW–SST (not shown). Thum et al. (2002) demonstrate from a simple calculation that this amount of anomaly in latent heat flux would produce $\sim 0.5^\circ\text{C}$ cooling of warm water, indicating a negative feedback to the TIW–SST. The present analysis of latent heat flux reveals, however, that, if these alternating positive and negative latent heat flux anomalies are averaged over the TIW period, a zonal cancellation makes the net contribution from the perturbations small compared to the mean contribution.

It should be emphasized that the TIWs do potentially rectify lower-frequency coupled variability through their contribution to the large-scale SST gradients (Jochum and Murtugudde 2006). Accumulation of small annual-mean perturbation heat and momentum fluxes could be important for the long-term climatic bias in SSTs and the equatorial current system in the tropical Atlantic Ocean (JMB). This low-frequency rectification must be revisited in much longer coupled simulations, but the focus here is on the rectification by the high-frequency atmospheric response to TIW-induced SST.

4. Summary and discussion

Ocean–atmosphere covariability arising in the presence of tropical instability waves (TIWs) was examined using a regionally coupled high-resolution climate model in the tropical Atlantic Ocean. One of the goals of the present study was to study the impact of the atmospheric wind response on the TIWs. Two mechanisms by which atmospheric wind fields feed back onto TIWs are a direct exchange of momentum and through a modification of wind stress curl.

Perturbations in the wind field are generated by undulating SST fronts of TIWs, which also produce a perturbation of surface currents. It was shown that these

wind perturbations and TIW-induced currents are negatively correlated over the TIW region. Thus, the perturbation surface winds are in the opposite direction to the surface currents, which slows down the TIW currents. In the EKE equation of the TIWs, this effect is a sink. At 2°N this energy sink amounts to $\sim 40\%$ of the barotropic conversion rate, which is the most dominant EKE source to the TIWs (JMB). If averaged over the TIW region (2°S–5°N), the wind contribution is roughly 10% of the barotropic conversion term.

Perturbations in wind stress curl are generated due to the TIW-induced SST gradient (Chelton et al. 2001). This wind stress curl generates perturbation Ekman pumping over the TIWs. Spall (2007) showed that Ekman pumping damps the baroclinic instability in the ocean in the presence of a southerly background wind. However, the present results suggest that in the case of Atlantic TIW Ekman pumping variability is negligible compared to the dynamically induced variability of upwelling. Thus, TIW-induced wind curl variations would not significantly modify baroclinic instability processes.

Furthermore, Ekman currents forced by the TIW-induced wind stress anomalies are many orders of magnitude smaller than the TIW currents (not shown). Thus, their impact on temperature will be negligible. This indicates that the variability of SST altered by already negligible TIW-induced Ekman currents is not important.

Overall, the atmosphere reduces the growth of TIWs by adjusting its wind variability according to the underlying TIW–SST field. This result corroborates the previous idealized modeling study by Pezzi et al. (2004), who implicitly includes these two atmospheric feedback mechanisms in their wind stress parameterization.

In addition, the effect of surface currents on wind stress magnitude is discussed. Over the large area across the equator in the tropical Atlantic Ocean, the ocean currents, including mean and TIWs, reduce surface wind stress estimates, with the maximum effects of 20% at 2°N, 20°W. This is because the westward South Equatorial Current is in the same direction as the large-scale atmospheric easterly flow (Pacanowski 1987).

In the annual mean, TIW currents only marginally rectify the wind stress estimates due to the oscillatory cancellation. However, at any time during the active TIW season, they can alter the local wind stress estimate by $\pm 25\%$ – 30% depending on the phase of the waves. Alternating phases of waves indicates that the peak-to-trough difference of surface stress may be even larger. This implies a potential for not only generating low-frequency rectification but also generating a mismatch between the TIWs simulated in forced ocean models with prescribed observed QuikSCAT

wind stresses. The inconsistency between these TIWs and the specified wind forcing when they are in the wrong phase may induce a spurious damping or strengthening of TIWs through the aforementioned coupling of the ocean current and the wind stress.

In such forced model simulations with the observed large-scale QuikSCAT wind forcing, one way to include the effect of coupling of wind and current would be to add, in the prescribed large-scale QuikSCAT forcing, spatially (and/or temporally) high-pass-filtered wind fields that are regressed on to the model's SST anomalies by TIWs. A test of this method would be to compare such forced ocean simulations with fully coupled simulations (such as with the SCOAR model). The results will provide a quantitative estimation of the potential impact of mismatch between the specified wind stress forcing and the model's TIWs.

Finally, the rectification effect of perturbations on the atmosphere due to TIWs is examined in terms of latent heat flux. A Reynolds averaging of the latent heat flux equation showed that zonal canceling of perturbation terms of wind speed and humidity differences gives rise to only a 1%–2% difference in latent heat flux compared to its mean contribution. This implies that, although negative feedback from heat flux response may be large at any given phase of SST, when integrated over TIW periods the perturbation heat flux will not significantly feed back on to the zonal-mean heat budget of the Atlantic Ocean.

Although our results suggest that TIW-induced latent heat flux does not rectify the mean SST on the short time scales, the TIWs still can operate over the larger-scale SST gradient to modulate the horizontal and vertical temperature advection that involves ocean–atmosphere heat and momentum exchanges (Jochum and Murtugudde 2006; Jochum et al. 2007). Moreover, there are studies that suggest a link between the interannual variability of the TIWs and the asymmetry of ENSO (e.g., Yu and Liu 2003). Long-term accumulation of small annual-mean perturbation heat and momentum fluxes may be important for the longer-term climatic bias in SSTs and currents in the tropical Atlantic Ocean. The potential low-frequency rectification of these apparently small feedbacks can be better quantified in much longer simulations of the coupled high-resolution model, which we are currently carrying out and will report elsewhere. This study is the first of its kind in addressing TIW feedback processes from a high-resolution full-physics coupled model.

Acknowledgments. The work was done during HS's visit to NCAR during summer 2006, which was made possible through a student fellowship of the Advanced

Study Program. This work forms a part of the Ph.D. dissertation of HS. This research was partially funded by NOAA Grant "Impact of oceanic mesoscale variability on the coupled climate" (NA17EC1483). We gratefully acknowledge additional funding support from DOE (DE-FG02-04ER63857) and NOAA (NA17RJ1231 through ECPC). The views expressed herein are those of the authors and do not necessarily reflect the views of these agencies. (The TMI data can be obtained from Remote Sensing Systems online at <http://www.ssmi.com>.)

REFERENCES

- Baturin, N. G., and P. P. Niiler, 1997: Effects of instability waves in the mixed layer of the equatorial Pacific. *J. Geophys. Res.*, **102**, 27 771–27 794.
- Brandt, P., F. A. Schott, C. Provost, A. Kartavtseff, V. Hormann, B. Bourlès, and J. Fischer, 2006: Circulations in the central equatorial Atlantic: Mean and intraseasonal to seasonal variability. *Geophys. Res. Lett.*, **33**, L07609, doi:10.1029/2005GL025498.
- Bryden, H. L., and E. C. Brady, 1989: Eddy momentum and heat fluxes and their effect on the circulation of the equatorial Pacific Ocean. *J. Mar. Res.*, **47**, 55–79.
- Chelton, D. B., and M. H. Freilich, 2005: Scatterometer-based assessment of 10-m wind analysis from the operational ECMWF and NCEP numerical weather prediction models. *Mon. Wea. Rev.*, **133**, 409–429.
- , and Coauthors, 2001: Observations of coupling between surface wind stress and sea surface temperature in the eastern tropical Pacific. *J. Climate*, **14**, 1479–1498.
- , M. G. Schlax, M. H. Freilich, and R. F. Milliff, 2004: Satellite measurements reveal persistent small-scale features in ocean winds. *Science*, **303**, 978–983.
- Conkright, M. E., R. A. Locarnini, H. E. Garcia, T. D. O'Brien, T. P. Boyer, C. Stephens, and J. J. Antonov, 2002: World ocean atlas 2001: Objective analysis, data statistics, and figures: CD-ROM documentation. National Oceanographic Data Center Internal Rep. 17, 21 pp.
- Cox, M. D., 1980: Generation and propagation of 30-day waves in a numerical model of the Pacific. *J. Phys. Oceanogr.*, **10**, 1168–1186.
- Cronin, M. F., S.-P. Xie, and H. Hashizume, 2003: Barometric pressure variations associated with eastern Pacific tropical instability waves. *J. Climate*, **16**, 3050–3057.
- da Silva, A. M., C. Young-Molling, and S. Levitus, 1994: *Atlas of Surface Marine Data 1994*. NOAA Atlas NESDIS 6-110, 83 pp.
- Dawe, J. T., and L. Thompson, 2006: Effect of ocean surface current on wind stress, heat flux, and wind power input to the ocean. *Geophys. Res. Lett.*, **33**, L09604, doi:10.1029/2006GL025784.
- Deser, C., J. J. Bates, and S. Wahl, 1993: The influence of sea surface temperature gradients on stratiform cloudiness along the equatorial front in the Pacific Ocean. *J. Climate*, **6**, 1172–1180.
- Düing, W., and Coauthors, 1975: Meanders and long waves in the equatorial Atlantic. *Nature*, **257**, 280–284.
- Eady, E. T., 1949: Long waves and cyclone waves. *Tellus*, **1**, 33–52.

- Fairall, C. W., E. F. Bradley, D. P. Rogers, J. D. Edson, and G. S. Young, 1996: Bulk parameterization of air-sea fluxes for Tropical Ocean-Global Atmosphere Coupled-Ocean Atmosphere Response Experiment. *J. Geophys. Res.*, **101**, 3747–3764.
- Haidvogel, D. B., H. G. Arango, K. Hedstrom, A. Beckmann, P. Malanotte-Rizzoli, and A. F. Shchepetkin, 2000: Model evaluation experiments in the North Atlantic Basin: Simulations in nonlinear terrain-following coordinates. *Dyn. Atmos. Oceans*, **32**, 239–281.
- Hansen, D., and C. A. Paul, 1984: Genesis and effects of long waves in the equatorial Pacific. *J. Geophys. Res.*, **89**, 10 431–10 440.
- Hashizume, H., S.-P. Xie, W. T. Liu, and K. Takeuchi, 2001: Local and remote atmospheric response to tropical instability waves: A global view from space. *J. Geophys. Res.*, **106**, 10 173–10 185.
- Hayes, S. P., M. J. McPhaden, and J. M. Wallace, 1989: The influence of sea surface temperature on surface wind in the eastern equatorial Pacific: Weekly to monthly variability. *J. Climate*, **2**, 1500–1506.
- Jochum, M., and R. Murtugudde, 2006: Temperature advection by tropical instability waves. *J. Phys. Oceanogr.*, **36**, 592–605.
- , P. Malanotte-Rizzoli, and A. Busalacchi, 2004: Tropical instability waves in the Atlantic Ocean. *Ocean Modell.*, **7**, 145–163.
- , M. F. Cronin, W. S. Kessler, and D. Shea, 2007: Observed horizontal temperature advection by tropical instability waves. *Geophys. Res. Lett.*, **34**, L09604, doi:10.1029/2007GL029416.
- Johns, W. E., T. N. Lee, R. C. Beardsley, J. Candela, R. Limeburner, and B. Castro, 1998: Annual cycle and variability of the North Brazil Current. *J. Phys. Oceanogr.*, **28**, 103–128.
- Juang, H.-M. H., and M. Kanamitsu, 1994: The NMC nested regional spectral model. *Mon. Wea. Rev.*, **122**, 3–26.
- , S.-Y. Hong, and M. Kanamitsu, 1997: The NCEP regional spectral model: An update. *Bull. Amer. Meteor. Soc.*, **78**, 2125–2143.
- Kalnay, E., and Coauthors, 1996: The NCEP/NCAR 40-Year Reanalysis Project. *Bull. Amer. Meteor. Soc.*, **77**, 437–471.
- Kanamaru, H., and M. Kanamitsu, 2007: Scale selective bias correction in a downscaling of global analysis using a regional model. *Mon. Wea. Rev.*, **135**, 334–350.
- Kanamitsu, M., and Coauthors, 2002a: NCEP dynamical seasonal forecast system 2000. *Bull. Amer. Meteor. Soc.*, **83**, 1019–1037.
- , W. Ebisuzaki, J. Woolen, S.-K. Yang, J. J. Hnilo, J. Potter, M. Fiorino, and G. L. Potter, 2002b: NCEP–DOE AMIP-II Reanalysis (R-2). *Bull. Amer. Meteor. Soc.*, **83**, 1631–1643.
- , H. Kanamaru, Y. Cui, and H. Juang, 2005: Parallel implementation of the regional spectral atmospheric model. NOAA PIER Project Rep. CEC-500-2005-014, 23 pp.
- Kelly, K. A., S. Dickinson, M. J. McPhaden, and G. C. Johnson, 2001: Ocean currents evident in satellite wind data. *Geophys. Res. Lett.*, **28**, 2469–2472.
- Legeckis, R., 1977: Long waves in the eastern equatorial Pacific Ocean: A view from a geostationary satellite. *Science*, **197**, 1177–1181.
- , W. Pichel, and G. Nesterczuk, 1983: Equatorial long waves in geostationary satellite observations and in a multichannel sea surface temperature analysis. *Bull. Amer. Meteor. Soc.*, **64**, 133–139.
- Lindzen, R. S., and S. Nigam, 1987: On the role of sea surface temperature gradients in forcing low-level winds and convergence in the Tropics. *J. Atmos. Sci.*, **44**, 2418–2436.
- Liu, W. T., K. B. Katsaros, and J. A. Businger, 1979: Bulk parameterization of air-sea exchanges of heat and water vapor including the molecular constraints at the interface. *J. Atmos. Sci.*, **36**, 1722–1735.
- , X. Xie, P. S. Polito, S.-P. Xie, and H. Hashizume, 2000: Atmospheric manifestation of tropical instability waves observed by QuikSCAT and tropical rain measuring mission. *Geophys. Res. Lett.*, **27**, 2545–2548.
- Luo, J.-J., S. Masson, E. Roeckner, G. Madec, and T. Yamagata, 2005: Reducing climatology bias in an ocean–atmosphere CGCM with improved coupling physics. *J. Climate*, **18**, 2344–2360.
- Masina, S., S. Philander, and A. Bush, 1999: An analysis of tropical instability waves in a numerical model of the Pacific Ocean 2. Generation and energetics of the waves. *J. Geophys. Res.*, **104**, 29 637–29 662.
- Pacanowski, R. C., 1987: Effect of equatorial currents on surface stress. *J. Phys. Oceanogr.*, **17**, 833–838.
- Pezzi, L. P., J. Vialard, K. J. Richard, C. Menkes, and D. Anderson, 2004: Influence of ocean–atmosphere coupling on the properties of tropical instability waves. *Geophys. Res. Lett.*, **31**, L16306, doi:10.1029/2004GL019995.
- Philander, S. G. H., 1976: Instabilities of zonal equatorial currents. *J. Geophys. Res.*, **81**, 3725–3735.
- , 1978: Instabilities of zonal equatorial currents, 2. *J. Geophys. Res.*, **83**, 3679–3682.
- Polito, P. S., J. P. Ryan, W. T. Liu, and F. P. Chavez, 2001: Oceanic and atmospheric anomalies of tropical instability waves. *Geophys. Res. Lett.*, **28**, 2233–2236.
- Proehl, H., 1996: Linear instability of equatorial zonal flows. *J. Phys. Oceanogr.*, **26**, 601–621.
- Qiao, L., and R. H. Weisberg, 1995: Tropical instability wave kinematics: Observations from the Tropical Instability Wave Experiment (TIWE). *J. Geophys. Res.*, **100**, 8677–8694.
- Schott, F. A., and Coauthors, 2003: The zonal currents and transports at 35°W in the tropical Atlantic. *Geophys. Res. Lett.*, **30**, 1349, doi:10.1029/2002GL016849.
- Seo, H., M. Jochum, R. Murtugudde, and A. J. Miller, 2006: Effect of ocean mesoscale variability on the mean state of tropical Atlantic climate. *Geophys. Res. Lett.*, **33**, L09606, doi:10.1029/2005GL025651.
- , A. J. Miller, and J. O. Roads, 2007: The Scripps Coupled Ocean–Atmosphere Regional (SCOAR) model, with applications in the eastern Pacific sector. *J. Climate*, **20**, 381–402.
- Shchepetkin, A. F., and J. C. McWilliams, 2005: The regional oceanic modeling system (ROMS): A split-explicit, free-surface, topography-following-coordinate ocean model. *Ocean Modell.*, **9**, 347–404.
- Small, R. J., S.-P. Xie, and Y. Wang, 2003: Numerical simulation of atmospheric response to Pacific tropical instability waves. *J. Climate*, **16**, 3723–3741.
- Spall, M. A., 2007: Effect of sea surface temperature–wind stress coupling on baroclinic instability in the ocean. *J. Phys. Oceanogr.*, **37**, 1092–1097.

- Thum, N., S. K. Esbensen, D. B. Chelton, and M. J. McPhaden, 2002: Air–sea heat exchange along the northern sea surface temperature front in the eastern tropical Pacific. *J. Climate*, **15**, 3361–3378.
- Wallace, J. M., T. P. Mitchell, and C. Deser, 1989: The influence of sea surface temperature on surface wind in the eastern equatorial Pacific: Seasonal and interannual variability. *J. Climate*, **2**, 1492–1499.
- Weisberg, R. H., 1984: Instability waves observed on the equator in the Atlantic Ocean during 1983. *Geophys. Res. Lett.*, **11**, 753–756.
- , and T. J. Weingartner, 1988: Instability waves in the equatorial Atlantic Ocean. *J. Phys. Oceanogr.*, **18**, 1641–1657.
- Xie, S.-P., 2004: Satellite observations of cool ocean–atmosphere interaction. *Bull. Amer. Meteor. Soc.*, **85**, 195–209.
- Yu, J.-Y., and W. T. Liu, 2003: A linear relationship between ENSO intensity and tropical instability wave activity in the eastern Pacific Ocean. *Geophys. Res. Lett.*, **30**, 1735, doi:10.1029/2003GL017176.
- Yu, Z., J. P. McCreary Jr., and J. A. Proehl, 1995: Meridional asymmetry and energetics of tropical instability waves. *J. Phys. Oceanogr.*, **25**, 2997–3007.
- Zhang, G. J., and M. J. McPhaden, 1995: The relationship between sea surface temperature and latent heat flux in the equatorial Pacific. *J. Climate*, **8**, 589–605.